Analyzing the Saturation of Growing Stem Volume Based on ZY-3 Stereo and Multispectral Images in Planted Coniferous Forest

Tingchen Zhang, Hui Lin, Jiangping Long, Meng Zhang, and Zhaohua Liu

***Abstract*—Recently, remote sensing (RS) technology are becoming an increasingly important technology in estimating forest growing stem volume (GSV), and the saturation issue of spectral variables from various optical sensors severely hinders the improvement of mapping forest GSV, especially in the planted forest with high GSV. Forest canopy height is widely considered as one of the major factors to increase the saturation levels in mapping GSV. However, it is rather difficult to invert the forest canopy height without precisely external DEM for large regions. In this study, the canopy height model (CHM) was derived from ZY-3 stereo images with subtracting open-sourced external DEM and the response of saturation levels was analyzed by adding forest height in the planted coniferous forest (Larch and Chinese pine). To further describe the relationships between the forest height and saturation levels, five datasets with five estimation models (Linear, MLR, SVR, KNN, and RF) and three methods of variable selection (Stepwise, LASSO, and Pearson) were applied to estimate the forest GSV using corrected CHM and 49 alternative variables extracted from ZY-3 multispectral images. Meanwhile, a spherical model was employed to quantitatively describe the saturation levels of combined variables. The results showed that values of relative root means square error were decreased from 29.3% to 25% for Larch and from 26.5% to 22.2% for Chinese pine after adding the corrected CHM, respectively. Meanwhile, the saturation level of each combined variable set was successfully determined by the spherical model. The results illustrated that the saturation levels of GSV were significantly increased by adding corrected CHM from open-sourced external DEM. Specially, the averaged saturation levels were increased from 220 m^3/ha to nearly 300 m^3/ha for Chinese pine and from 150 m^3/ha to 220 m^3/ha for Larch, respectively. It is proved that ZY-3 stereo and multispectral images have great potential for accurate estimation of forest GSV by delaying the saturation levels using extracted CHM with open-sourced external DEM.**

Manuscript received August 8, 2021; revised October 10, 2021 and November 17, 2021; accepted November 29, 2021. Date of publication December 1, 2021; date of current version December 20, 2021. This work was supported in part by the National Key R&D Program of China project "Research of Key Technologies for Monitoring Forest Plantation Resources" under Grant 2017YFD0600900 and in part by Innovative province and Construction special funds of Hunan Province "Intelligent measurement and monitoring technology of forest stock, biomass and carbon storage based on multi-source data of land, space and sky" under Grant 2020NK2051. *(Corresponding author: Jiangping Long.)*

The author are with the Research Center of Forestry Remote Sensing & Information Engineering, Central South University of Forestry and Technology, Changsha 410004, China, with the Hunan Key Laboratory of Forestry Remote Sensing Big Data and Security, Changsha 410004, China, and also with the Key Laboratory of Forest Resources Management and Testing in Southern China, National Forestry and Grassland Administration, Changsha 410004, China (e-mail: 1097863780@qq.com; linhui@csuft.edu.cn; t20080976@csuft.edu.cn; mengzhang@csuft.edu.cn; 20171100032@csuft.edu.cn).

Digital Object Identifier 10.1109/JSTARS.2021.3131812

***Index Terms*—Canopy height model (CHM), growing stem volume (GSV), saturation, spherical model, ZY-3.**

I. Introduction

GLOBAL warming is one of the biggest challenges faced by mankind and forest plays an important role in carbon dioxide emissions and global climate change [1]–[3]. Naturally, forest growing stem volume (GSV) is regarded as one of the key parameters to evaluate the quality of forest resources. Although traditional field-based forest inventory can provide relatively accurate GSV on sample scale, the process is time-consuming and labor-intensive, and in some cases, access to certain remote forest areas is impossible [4]. At present, remote sensing (RS) technology is becoming an increasingly important tool for estimating GSV and resource assessment [5]–[8]. Over the last few decades, many variables related to forest GSV were extracted from optical RS images with multispatial resolutions and multispectral (Mul-SP) sensors, such as Landsat series, Sentinel-2, GF series, and ZY series satellites [9]–[14]. Meanwhile, the saturation levels of GSV have been found using various RS images [19]. Furthermore, the common problem is also recognized for mapping GSV or AGB using SAR images [20]–[22]. The phenomenon of spectral saturation varies with various spectral, spatial, and radiometric resolutions [17], [18]. Additionally, tree species and forest with different stand structures also induced various saturation levels [23], [24]. Thus, how to delay the saturation levels is an unavoidable problem for improving the accuracy of mapping forest GSV using optical RS images [25].

Facing the challenge of spectral saturation, the models and RS images are initially considered to increase the saturation levels [26], [27]. Excepting the linear and nonlinear models, several complex machine learning and deep learning algorithms, such as support vector machine model (SVR) [28], [29], random forest (RF) model [30], K-nearest neighbor (KNN) method [31], CNN, and ensemble learning algorithms, are often employed to map GSV in various forest and the results showed that these models can improve the accuracy of GSV by delaying the saturation. The other methods are mainly concentrated in RS data by various combined variables derived from multitemporal images or multisource images [32].

Moreover, it is noted that the forest canopy height is widely considered as one of the main factors to increase the saturation levels in estimation GSV. Normally, the forest height

(also named CHM, canopy height model) related to GSV is mainly derived from airborne laser scanning technology [6], [33], and then three-dimensional point clouds and precise DEM enable to extract the reliable CHM and GSV in local regions [25], [34]. Meanwhile, the results of using C and L band polarimetric SAR images to estimate forest height show that the saturation level of plantation forests can be effectively delayed [35]–[38]. However, with the expensive of acquired data, it is difficult to be widely applied to map forest GSV on large scales [39], [40]. Considering the cost of acquired data, digital surface model (DSM) can be also derived from spaceborne stereo images (worldview 2 and ZY3) for large regions [41], [42]. In previous, forest AGB was mapped by using difference of DSM at leaf-on and leaf-off seasons extracted from the ZY-3 stereo images. Moreover, the forest height was also extracted by a combination of lidar-based DEM and stereo-based DSM extracted from stereo images. However, it is still difficult to extract the reliable CHM from stereo images without precise DEM [4].

On the other hand, the saturation phenomenon of optical images has been recognized for a long time, it is still a hot disputed problem to construct the models for quantitatively describing the saturation levels based on various forest types and images [25]. At present, both nonparameters and parameters approaches are employed to determinate saturation levels of various images and forest types [43], [44]. For the nonparameters approach, the saturation levels were indirectly obtained by visually interpreting the extreme values of linear models or the trends of nonlinear models based on scatterplots or fitted curves between selected variables and GSV [45]. For the parameters approach, the saturation level was regarded as one of the parameters. The semiexponential model is traditional parameters approach for estimating the saturation levels using polarmetric SAR images, and the saturation level is one parameter of the model directly derived from solving the models [27], [46]. Additionally, it has been found that the principle of the kriging model based on the semicovariance function in geostatistics is similar to the phenomenon of spectral saturation, and a spherical model is also used to quantitatively estimate the saturation values of AGB using spectral reflectance from Landsat imagery, and the results indicated that the saturation levels of AGB highly related to forest types and slope aspects [13], [14]. In fact, for a single variable, both nonparameters and parameters approaches have the capability to quantitatively evaluate the saturation levels by extreme values or solving models. However, it is still a complex problem to evaluate the saturation of combined variables applied in the machine learning and deep learning algorithms.

Therefore, the goal of the present study is to quantitatively describe the saturation levels of combined variables by general spherical model and to investigate the potential capability to delay the saturation levels using stereo images with open-sourced external DEM [15]. In the study area, a pair of ZY-3 images with the spatial resolution of 2.1 m, including forward image, backward image, and nadir image (Mul-SP images), were employed to map GSV in planted coniferous forest (Larch and Chinese pine) [3], [13], [47]. And then, the CHM was extracted from stereo images and open-sourced external DEM [48]. Meanwhile, the spherical model was used to quantitatively evaluate the saturation levels of various combined variables extracted from ZY-3 stereo and Mul-SP images [49].

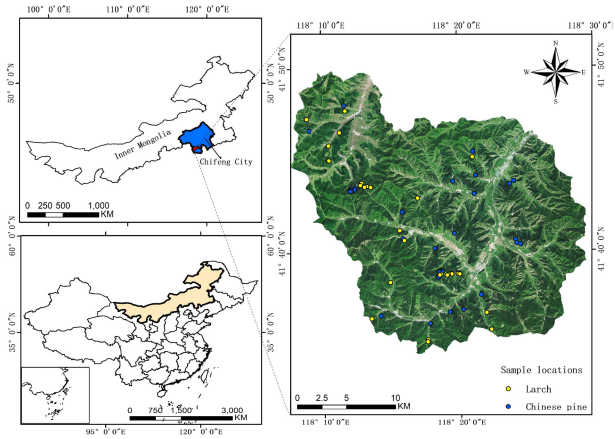

Fig. 1. Study area and ground plots.

II. Materials and Methods

A. Study Area

Wangyedian Experimental Forest Farm (118°09'E–118°30'E, 41°21'N–41°39'N) is in the southwest of Harqin Banner, Chifeng City, Inner Mongolia, China (see Fig. 1). The landforms of the study area are mainly mountainous regions with elevation varying from 600 to 1890 m. There are four soil types, including brown soil, cinnamon soil, meadow soil, and mountain black soil, and the brown soil is the mainly one. The forest area was up to 23 300 hectares and the percentage forest cover was about 93% by the end of 2016, with a total stock volume of 1.527 million m^3. About 49.78% of the study area (about 11 600 hectares) is covered by planted forest and the main tree species are larch (*Larix principis-rupprechtii and Larixolgensis*) and Chinese pine (*Pinus tabuliformis*) in the planted forest.

B. Ground Data and RS Images

1) Ground Data: Based on the distribution of GSV in planted coniferous forest, 35 larch plots and 32 Chinese pine plots with the size of 25 m × 25 m were measured in September 2017 by the approach of random stratification sampling (see Fig. 1). The positions of corners and central points in each plot were precisely measured by the Global position system. And then, the parameters of each tree with the diameter at breast height (DBH) larger than 5 cm, such as height, DBH, and size of canopy, were measured and the timber volume of each tree was calculated using the equations related to the measured height and DBH. For the Larch and Chinese pine, the equations of timber volume provided by Wangyedian forest farm were developed in accordance with the technical regulations on the construction of two-variable tree volume table of the People's Republic of

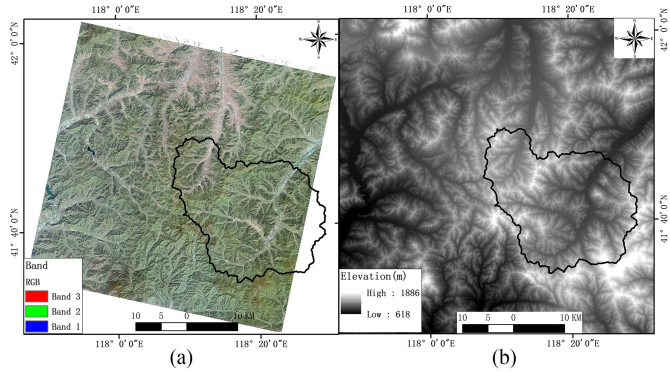

Fig. 2. (a) ZY-3 Mul-SP images acquired on September 20, 2017. (b) DEM of the study area.

China (bz0000008300)[1] [50]

$$\text{Larch}: V = -0.001498 + 0.00007 \times D^2 + 0.000901 \times H + 0.000032 \times H \times D^2 \quad (1)$$

$$\text{Chinese pine}: V = 0.013464 - 0.001967 \times D + 0.000089 \times D^2 + 0.000628 \times D \times H + 0.000032 \times H \times D^2 - 0.003173 \times H \quad (2)$$

where V is the volume of each tree, H and D are the height and DBH of each tree. The GSV of ground plot was the sum of all the tree timber volume within the plot. In the study, the GSV of Larch samples varied between 86.17 and 405.56 m^3/ha and the average GSV was 208.42 m^3/ha; the GSV of Chinese pine samples varied between 91.97 and 355.61 m^3/ha and average GSV was 212.18 m^3/ha.

2) RS Data and Preprocessing: Because of the availability of Mul-SP and stereo images, the Ziyuan-3 (ZY-3) satellite data are widely used to invert the digital elevation model (DEM) without forest on large scale. In our study, one pair of stereo images with a spatial resolution of 2.1 m was acquired on September 20, 2017 [see Fig. 2(a)], and the DSM was generated. Moreover, for extracting the CHM, the open-sourced DEM with a resolution of 12.5 m was downloaded from NASA-EARTHDATA[2] [see Fig. 2(b)].

After processing of atmospheric calibration, the topographic correction was also processed by the C-correction model to reduce the influence of steep slope terrains. And then, to avoid problems of overconcentration of certain band information, the Gram–Schmidt fusion method was used to fuse the multispectral and panchromatic data to produce a new image with a spatial resolution of 2.1 m [51], [52]. So, the fused Mul-SP images were used to extract the spectral variables for GSV inverting.

C. Extracting CHM From ZY-3 Stereo Images

By three high-resolution panchromatic cameras, the three images, forward, nadir, and backward image were used to provide the in-orbit stereo images pair. OrthoMapping tool of ArcGIS 10.5 software was used to derive the DSM from ZY-3 stereo images [47]. To accurately retrieve the DSM from ZY-3 stereo images, calculating connection points was the first step. And then, the regional network adjustment was used to construct the geometry relationships of the same image points picked out from stereo images. After that, the stereo pair was reconstructed to produce the model of point clouds, and the DSM was successfully extracted after matching and interpolating. To match the resolution of DEM, the extracted DSM and open-sourced DEM were both resampled to a resolution of 20 m, and then CHM is calculated by subtracting DEM from DSM (see Fig. 3) [53], [54].

TABLE I
LIST OF VARIABLES EXTRACTED FROM ZY-3 MULTISPECTRAL IMAGES

Variables	Definition method
Original band	*band 1 - BLUE, band 2 - GREEN, band 3 - RED, band 4 - NIR*
NDVI	*NDVI = (NIR − RED) / (NIR + RED)*
DVI	*DVI= NIR - RED*
RVI	*RVI= NIR / RED*
EVI	*EVI =2.5×(NIR−RED)/(NIR+6×RED−7×BLUE+1)*
ARVI	*ARV I = (NIR−(2×RED− BLUE)) / (NIR +(2×RED–BLUE))*
SAVI	$SAVI_i = (NIR - RED)(1+p)/(NIR + RED + p)$, p=0.25,0.5,0.75
TVI	*0.5×(120×(NIR−GRN) − 200×(RED−GRN))*
MSR	*MSR=(NIR/RED-1)/SQRT(NIR/RED+1)*
NLI	*NLI=(NIR*NIR-RED)/(NIR*NIR+RED)*

D. Extraction the Variables and Variables Selection

For mapping the GSV of planted coniferous forest, alternative variables of four bands, nine vegetation indices, and eight texture characteristics were extracted from preprocessed ZY-3 Mul-SP images, and some topographic variables were extracted from DEM. Normally, nine vegetation indices included Normalized Differential Vegetation Index (NDVI), Difference Vegetation Index (DVI), Ratio Vegetation Index (RVI), Enhanced Vegetation Index (EVI), Atmospheric Impedance Vegetation Index (ARVI), Soil Regulation Vegetation Index (SAVI0.25, SAVI0.5, SAVI0.75), Triangular Vegetation Index (TVI), Modified Simple Index (MSR), and NLI (see Table I). Moreover, the eight texture variables were extracted from each selected band with the size of 3×3 [18], [19]. Additionally, the slope and aspect variables were extracted from DEM. To select the key variables from extracted 49 alternative variables, three methods of variables selection, including Pearson correlation coefficient, LASSO model, and stepwise regression model, were adopted in the next step [50], [55], [56].

E. Estimation Models for Corrected CHM, GSV, and Saturation Levels

1) Estimation Models of Corrected CHM and GSV: For reducing the errors of CHM, the extracted CHM should be

[1][Online]. Available: http://www.forestry.gov.cn/portal/xdly/s/5191/content-973771.html

[2][Online]. Available: https://search.asf.alaska.edu/

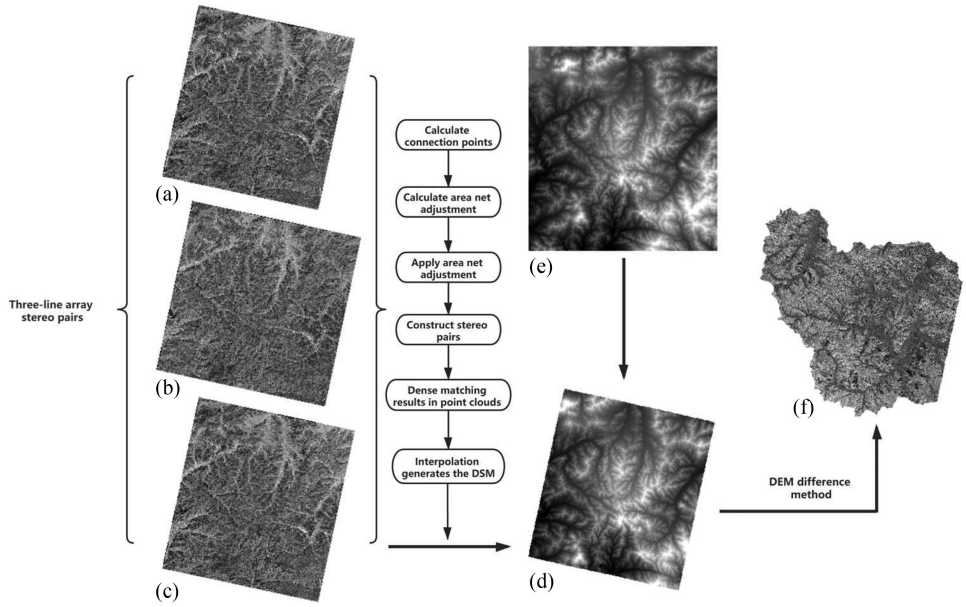

Fig. 3. Flow chart of generation CHM. (a) ZY-3 forward view image. (b) ZY-3 nadir image. (c) ZY-3 back view image. (d) ZY-3 three-view DSM. (e) Open-sourced external DEM. (f) CHM of study area.

corrected by field-measured forest height in plots and variables extracted from ZY-3 Mul-SP images. In our study area, four models, such as multiple linear regression model (MLR), SVR model, RF model, and KNN method, were selected to estimate the corrected CHM (CCHM). And then, those models (MLR, SVR, RF, and KNN) were also employed to invert the GSV using CCHM from stereo images and variables from ZY-3 Mul-SP images and DEM.

To evaluate the estimated results of the CCHM and GSV, the leave-one-out cross-validation (LOOCV) was employed to calculate the root means square error (RMSE) and the coefficient of determination (R^2) between the estimated and the observed values. The relative RMSE (rRMSE) was also utilized for the accuracy assessment. The formulas of the three indices were listed as following:

$$R^2 = 1 - \frac{\sum_{i=1}^{\mathrm{n}} \left(\mathrm{y_i} - \hat{\mathrm{y}}_\mathrm{i}\right)^2}{\sum_{i=1}^{\mathrm{n}} \left(\mathrm{y_i} - \bar{\mathrm{y}}\right)^2} \tag{3}$$

$$\mathrm{RMSE} = \sqrt{\frac{\sum_{i=1}^{\mathrm{n}} \left(\mathrm{y_i} - \hat{\mathrm{y}}_\mathrm{i}\right)^2}{n}} \tag{4}$$

$$r\mathrm{RMSE} = \mathrm{RMSE}/\overline{y} \times 100\% \tag{5}$$

where $\widehat{y}$ and y are the estimated and ground measured GSV or CHM, respectively.

2) Approach for Evaluating the Saturation Level: When the GSV reached at a certain value, the saturations of spectral variables would occur. So, it is hard to estimate the forest GSV exceeded the saturation level. Therefore, how to evaluate the saturation value is important for improving the accuracy of GSV. It is reported that the saturation phenomenon of interested variables is similar to the distribution of spatial autocorrelation of a variable of interest in geostatistics [14], [57]. And the approach of the semi-variogram model was selected to evaluate the saturation level and express the relationship between forest GSV and the selected spectral variables. In this study, a spherical model is used to solve the semi-variance function, and the specific formula is as follows:

$$f(h) = \begin{cases} 0 & h = 0 \\ c_0 + c\left(\frac{3h}{2a} - \frac{h^3}{2a^3}\right) & 0 < h < a \\ c_0 + c & h > a \end{cases} \tag{6}$$

where c_0 is the nugget constant, c is the arch height, c_0+c is the abutment value, and a is the variable range; when c_0= 0, c = 1, it is called the standard spherical model. When $y = f(h)$, b_0=c_0, b_1=3c/2a, b_2=$\mathrm{c}^3/2\mathrm{a}^3$, h=x, the model is obtained:

$$y = b_0 + b_1 x + b_2 x^3 \tag{7}$$

where y is the selected variable value and x is the GSV of the ground plot. The solution of unknown parameters, b_0, b_1, and b_2, were retrieved by the least squares algorithm and the values of saturation level were determined by the extremum of the spherical model. For a variable, the ground measured forest GSV was regarded as spatial distance in geo-statistics, and the level of saturation values is directly extracted by the extremum of the spherical model. However, it is difficult to evaluate the saturation level of the variable set by the spherical model.

To evaluate the saturation level of GSV with multivariables, the variable of the red band from ZY-3 Mul-SP images was selected as a response variable attributed to spatial autocorrelation, and the estimated forest GSV from combined variables was selected to solve the spherical model [13], [58]–[60]. And then, the saturation of combined variables is illustrated by the relationship between the red band and estimated GSV. Basically, the saturation level of each combined variable is dependent indirectly on the combined variables and estimated model.

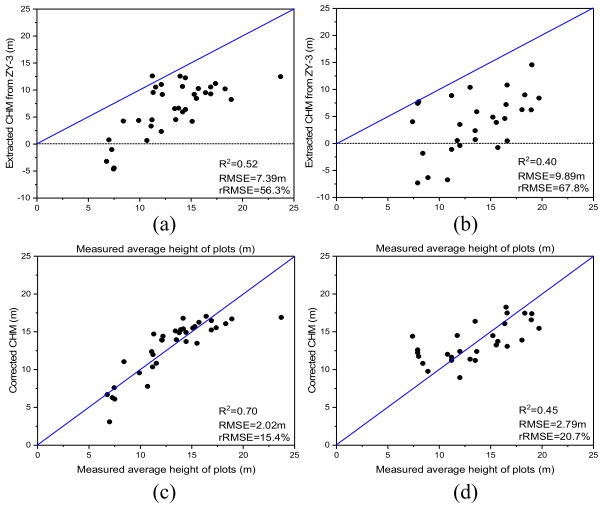

Fig. 4. Scatter graphs between CHM extracted from ZY-3 stereo images and measured average height of plots; (a)–(b) Scatters between extracted CHM and measured average height of plots for Larch and Chinese pine, respectively. (c)–(d) Scatters between CCHM and measured average height of plots for Larch and Chinese pine, respectively.

III. Results

A. Results of Extracted Forest Height

Fig. 4(a) and (b) showed the scatter graphs between the extracted CHM from ZY-3 stereo images and measured average height of plots for Larch and Chinese pine, respectively. Because of errors of imaging and open-sourced DEM, the directly extracted CHM were obviously lower than the measured average height of plots. To reduce the errors of CHM, the models between the extracted CHM, measured average height of plots, and spectral variables were constructed using three approaches of variable selection and four employed models, and the results of CCHM were listed in Table II.

As shown in Table II, the values of the determination coefficient (R^2) were ranged from 0.43 to 0.70 for Larch and from 0.14 to 0.45 for Chinese pine, respectively. For Larch plots, the minimum RMSE (2.02 m) between the CCHM and ground measured average height of samples was obtained by the MLR model with a stepwise regression approach for variable selection. And the optimal result of Chinese pine was extracted from the RF model under the LASSO approach. Moreover, the accuracy of CCHM for Larch was higher than that for Chinese pine.

Fig. 4 compared the scatter graphs between the extracted CHM and CCHM. Before applying the correcting model [see Fig. 4(a) and (b)], the RMSE between directly extracted CHM and measured GSV were 7.39 and 9.89 m, and rRMSE were 56.3% and 67.8%, for Larch and Chinese pine, respectively. After correcting [see Fig. 4(c) and (d)], the underestimated heights of plots were significantly decreased, and the RMSE between CCHM and measured GSV were up to 2.02 m for Larch and 2.79 m for Chinese pine, and rRMSE were up to 15.4% and 20.7%, respectively. It was shown that the CCHM was more sensitive to the changes of GSV than directly extracted CHM. And then, the optimal estimating models and variable selection method were employed to obtain the correction CHM of study area.

TABLE II
Results of CCHM Extracted From Various Methods of Variable Selection and Models

Tree special	Variable selection	Model	R^2	RMSE (m)	rRMSE (%)	Note
Larch	Pearson	MLR	0.46	2.74	20.9	
		SVR	0.63	2.29	17.5	
		RF	0.63	2.29	17.4	*
		KNN	0.45	2.76	21.0	
	LASSO	MLR	0.67	2.13	16.3	*
		SVR	0.57	2.45	18.7	
		RF	0.67	2.14	16.3	
		KNN	0.41	2.66	22.3	
	Stepwise regression	MLR	0.70	2.02	15.4	*
		SVR	0.53	2.56	19.5	
		RF	0.57	2.46	18.7	
		KNN	0.43	2.82	21.5	
Chinese pine	Pearson	MLR	0.21	3.34	24.8	
		SVR	0.30	3.14	23.3	*
		RF	0.28	3.17	23.6	
		KNN	0.17	3.61	26.8	
	LASSO	MLR	0.33	3.06	22.7	
		SVR	0.25	3.25	24.1	
		RF	0.45	2.79	20.7	*
		KNN	0.40	2.91	21.6	
	Stepwise regression	MLR	0.36	2.99	22.2	*
		SVR	0.27	3.21	23.8	
		RF	0.25	3.25	24.1	
		KNN	0.14	3.66	27.1	

Note: * in the above table is the optimal model for each method.

B. Results of Estimated GSV

1) Variable Selecting for Estimating GSV: To investigate the saturation level of GSV in the study area, 49 alternative variables were extracted from ZY-3 Mul-SP images. In our study, three methods of variable selection (Pearson coefficients, LASSO, and stepwise regression) were applied to select the optimally combined variables for GSV estimation. Based on each approach, the top ten variables of each method were listed in Table III. It was shown that most of the variables related to vegetation indices were selected for Larch and most of the variables related to texture characteristics were selected for Chinese pine. Additionally, to determine the number of variables for GSV estimation, the threshold values of Pearson correlation were set to 0.6 for Larch and 0.4 for Chinse pine.

2) GSV Estimation: To evaluate the ability of variables for GSV estimation, there were five types of variable set extracted from ZY-3 stereo and Mul-SP images using three methods of variables selection, including CHM, CCHM, selected Mul-SP variables, combined variables between extracted CHM and selected Mul-SP variables (Mul-SP-CHM), and combined variables between CCHM and selected Mul-SP variables (Mul-SP-CCHM). And then, five models, linear model, MLR SVR model, RF model, and KNN method, were employed to estimate the GSV in each type of selected variables. Furthermore, the linear

TABLE III
RESULTS OF VARIABLE SELECTION BY THREE APPROACHES

	Pearson correlation			LASSO		Stepwise regression	
	Name of variables	Rank	Correlation coefficient	Name of variables	Rank	Name of variables	Rank
Larch	ARVI	1	0.715**	DVI	1	ARVI	1
	TVI	2	0.705**	RVI	2	TVI	2
	NDVI	3	0.704**	EVI	3	EVI	3
	SAVI0.25	4	0.704**	B2_VA	4	NDVI	4
	SAVI0.5	5	0.704**	ARVI	5	SAVI0.25	5
	EVI	6	0.695**	B3_HO	6	SAVI0.5	6
	MSR	7	0.692**	B2_ME	7	B3_VA	7
	RVI	8	0.684**	B3_DI	8	DVI	8
	NLI	9	0.568**	B4_HO	9	B4_HO	9
	B2_HO	10	0.375*	Band3	10	Band2	10
Chinese pine	B4_SM	1	0.433**	B2_ME	1	B3_DI	1
	B2_ME	2	-0.419**	B3_ME	2	B2_ME	2
	B3_DI	3	0.418**	B3_DI	3	B3_CT	3
	B1_ME	4	-0.410**	B4_VA	4	B2_CT	4
	B4_VA	5	-0.408**	B4_EN	5	B2_VA	5
	B4_CO	6	0.388**	Band3	6	B3_VA	6
	B4_ME	7	-0.384**	Band4	7	B4_ME	7
	B3_ME	8	-0.381**	B1_ME	8	B4_VA	8
	B4_HO	9	0.366*	B2_DI	9	B2_SM	9
	B2_HO	10	0.365*	B2_VA	10	B2_DI	10

Note: ** in the above table is significantly correlated at the 0.01 level (two-sided), and * is significantly correlated at the 0.05 level (two-sided).

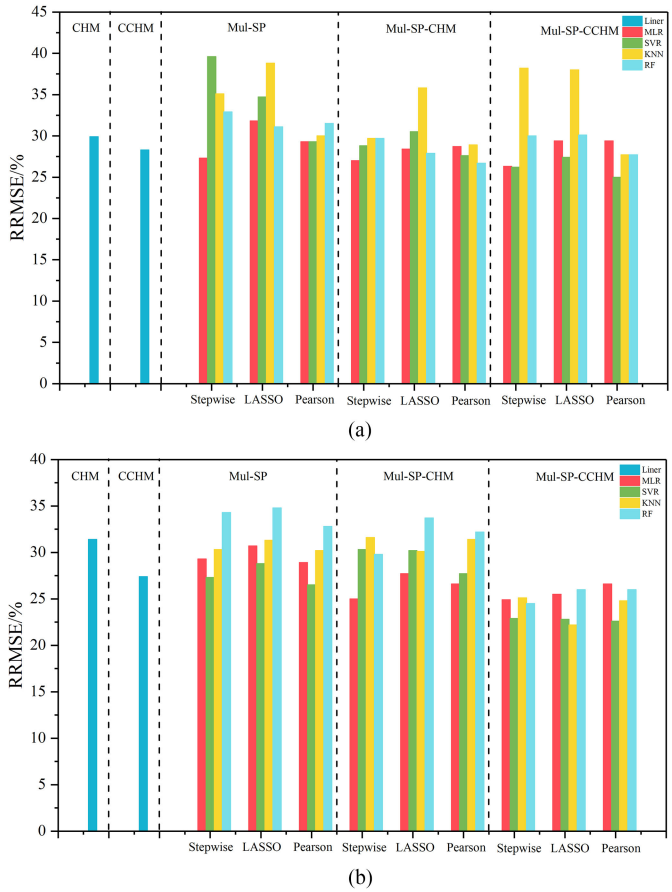

Fig. 5. Histograms of rRMSE calculated by three variable selection methods and five combined variable sets. Stepwise, LASSO, and Pearson are methods for variable selection, CHM indicates directly extracted canopy height model, CCHM indicates CCHM, M indicated Mul-SP variables, M-CHM indicates CHM and Mul-SP variables, M-CCHM indicates CCHM and Mul-SP variables.

model was directly used to the single variable of CHM and CCHM and others were applied to the combined variable set. The method of LOOCV was utilized for the accuracy assessment, and the values of RMSE and rRMSE were used to evaluate the results of the estimated GSV. The histograms of rRMSE were shown in Fig. 5(a) and (b).

As shown in Fig. 5, the values of rRMSE (Larch: 29.9% and Chinese pine: 31.4%) from extracted CHM were larger than that from CCHM (Larch: 28.3% and Chinese pine: 27.4%). Among the other four models in three types of combined multivariables, the values of rRMSE from KNN for Larch were larger than that from other models, and the values of rRMSE from RF for Chinese pine were larger than those from other models. Moreover, by adding the variables of CHM, the values of rRMSE from combined variables were much smaller than that from Mul-SP variables. Table IV lists the optimal results from three methods of variable selection and five estimated models in each type of selected variable. The determination coefficient (R^2) is ranged from 0.41 to 0.62 for Larch and from 0.18 to 0.59 for Chinese pine, respectively. Moreover, the smallest RMSE and rRMSE were 52.3 m^3/ha and 25.0% for Larch, obtained by the model of SVR and variables selection method of Pearson in combined variables between CCHM and Mul-SP variables. Meanwhile, the rRMSE from combined variables (M-CCHM) were greatly decreased by adding the CCHM for larch and Chinese pine in the study area. It is inferred that the errors of estimated GSV were reduced by adding the variable of CHM.

To further analyze the results of the estimated GSV, Fig. 6 illustrated the scatter graphs between measured and predicted GSV from the optimal model of each type of combined variable. It often occurred that the plots with low GSV were overestimated and the plots with high GSV were underestimated without using the CHM [see Fig. 6(c) and (h)], and these overestimated or underestimated plots were significantly decreased by adding CHM [see Fig. 6(d), (e), (i), and (j)]. Furthermore, the results of the estimated GSV by adding the CCHM were more sensitive than that by adding the CHM. So, it is proved that the CHM has the potential ability to improve the results of high GSV by delaying the saturation level.

Using selected the optimally combined variables by Pearson for Larch and by LASSO for Chinese pine, the GSV of the study area was mapped by the optimal model of SVR for Chinese Pine [see Fig. 7(a)] and KNN for Larch [see Fig. 7(b)], respectively. As shown in Fig. 7, the estimated GSV of Chinese pine (mainly ranged from 150 to 250 m^3/ha) was higher than that of Larch (mainly ranged from 100 to 150 m^3/ha).

C. *Saturation Levels of GSV*

Normally, the accuracy of GSV is highly related to saturation levels of variables, especially in high GSV areas. It is necessary

TABLE IV
OPTIMAL RESULTS OF ESTIMATED GSV FROM FOUR MODELS IN EACH METHOD OF VARIABLE SELECTION

Tree species	Variables	Variable selection	Models	R^2	RMSE(m^3/ha)	rRMSE (%)	Note
Larch	CHM	-	linear	0.45	62.3	29.9	
	CCHM	-	linear	0.51	59.0	28.3	
	Mul-SP	Stepwise regression	MLR	0.54	57.0	27.3	
		LASSO	RF	0.41	64.7	31.1	
		Pearson	MLR	0.47	61.1	29.3	*
	Mul-SP-CHM	Stepwise regression	MLR	0.55	56.4	27.0	
		LASSO	RF	0.52	58.1	27.9	
		Pearson	RF	0.57	55.7	26.7	*
	Mul-SP-CCHM	Stepwise regression	SVR	0.58	54.5	26.2	
		LASSO	SVR	0.54	57.1	27.4	
		Pearson	SVR	0.62	52.3	25.0	*
Chinese pine	CHM	-	linear	0.18	69.2	31.4	
	CCHM	-	linear	0.38	60.4	27.4	
	Mul-SP	Stepwise regression	SVR	0.38	60.2	27.3	
		LASSO	SVR	0.31	63.5	28.8	
		Pearson	MLR	0.42	58.5	26.5	*
	Mul-SP-CHM	Stepwise regression	MLR	0.48	55.2	25.0	*
		LASSO	MLR	0.36	61.1	27.7	
		Pearson	MLR	0.41	58.6	26.6	
	Mul-SP-CCHM	Stepwise regression	RF	0.50	54.0	24.5	
		LASSO	KNN	0.59	48.9	22.2	*
		Pearson	SVR	0.57	49.9	22.6	

Note: * in the above table is the optimal model for each method.

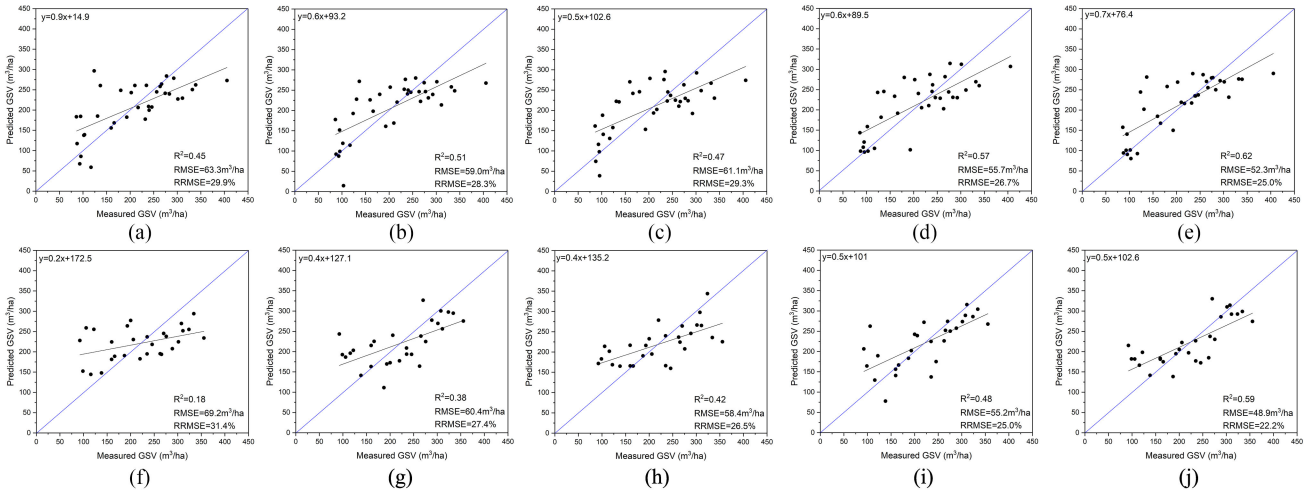

Fig. 6. Scatter graphs between measured and predicted GSV from the optimal model of each type of combined variables. (a)–(e) Optimal results from CHM, CCHM, Mul-SP variables (Mul-SP), Mul-SP-CHM, and Mul-SP-CCHM for Larch, respectively. (f)–(j) Optimal results from CHM, CCHM, Mul-SP variables (Mul-SP), Mul-SP –CHM, and Mul-SP -CCHM for Chinese pine, respectively.

to explore the change of saturation after adding CHM. As shown in Fig. 6 and Table IV, it was illustrated that the accuracy of estimated GSV depends on the selected combined variables, employed models, and forest stand structures. The capability of combined variables and models for estimating GSV, especially for high GSV areas, is mainly related to saturation levels. Fig. 8 illustrated the scatter graphs between variable of red band extracted from ZY-3 Mul-SP images and ground measured GSV, the saturation of the variable was obviously occurred at the level of 150 m^3/ha for Larch and 220 m^3/ha for Chinese pine (Blue line), respectively. So, the accuracy of estimated GSV was decreased by underestimated results.

In the study, the approach of spherical model was selected to evaluate the saturation level and express the relationship between forest GSV and the selected variables. Compared with a single spectral variable, the saturation levels of GSV were obviously increased by using combined variables. To quantitatively describe the saturation levels of combined variables, the values

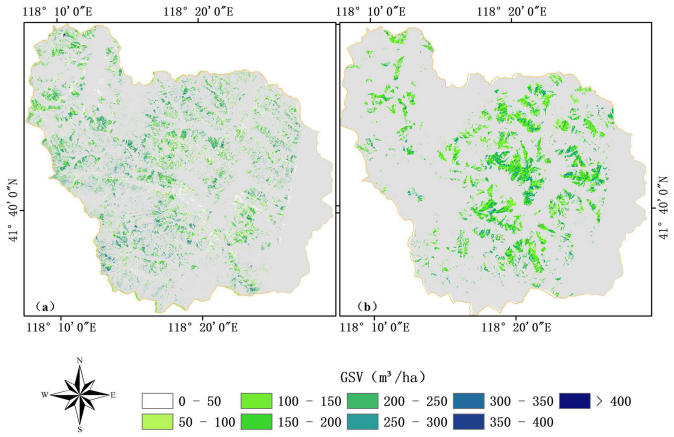

Fig. 7. Map of GSV for larch and Chinese pine in the study area. (a) Map of GSV for Larch from the model of SVR with combined variables of Mul-SP-CCHM and Pearson. (b) Map of GSV for Chinese pine from the model of KNN with combined variables of Mul-SP-CCHM and LASSO.

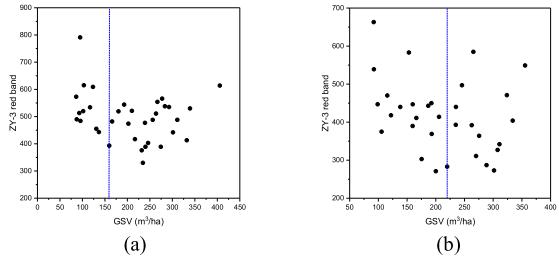

Fig. 8. Scatter graphs between the variable of red band extracted from ZY-3 multispecial images and ground measured GSV. (a)–(b) Scatter graphs for Larch and Chinese pine, respectively.

of red band extracted from ZY-3 Mul-SP images was regarded as a response variable, and estimated GSV of ground plots was regarded as independent

variables. After obtaining the estimated GSV, the values of saturation were determined by spherical model for the single and combined variable set. Based on the results in Table IV, the optimal estimated GSVs for each type of combined variable were used to solve the parameters of spherical model. Then, the minimum values of curves were obtained to extract the saturation levels. Table V listed the obtained saturation levels of single and combined variables from the optimal estimated GSV. For the single variable of red band, the saturation levels of GSV were close to 150 m^3/ha for Larch and 220 m^3/ha for Chinese pine, and the values were up to 192 m^3/ha for Larch and 270 m^3/ha for Chinese pine using combined variable from Mul-SP images. Furthermore, the saturation level was significantly delayed by using a single CHM from ZY-3 stereo images. After combining the CCHM with Mul-SP variables, the obtained saturation levels were up to 266 m^3/ha for Larch and 207 m^3/ha for Chinese pine, respectively. To further describe the capability for estimating GSV, the curves of the spherical model were shown in Fig. 9. By adding the CHM, the minimum of the curves moves to the direction with higher GSV. So, the accuracy of the estimated GSV was increased by the combined variables with high levels of saturation.

IV. Discussion

A. CHM Related to Estimated GSV

Generally, a reliable estimation of forest GSV requires not solely information extracted from optical spectral images, the forest height is also an important parameter to describe the volume of a single tree. Traditionally, airborne laser scanning and stereo images are mainly data for obtaining the forest height. Earlier, the stereo images from varied platforms, such as worldview, Quickbird, GeoEye-1, have been employed to quantify DSM and forest GSV [4], [54]. Normally, the accuracy of extracted CHM depends on the DSM derived from stereo images and DEM from other sources. For forested regions, the coincident external DEM without forest canopy height is often unavailable or spatially limited. In our study, the open-sourced DEM with a resolution of 12.5 m was employed from NASA-EARTHDATA. So, there are some issues for extracting the reliable CHM and forest GSV, concluding the inconsistency between the stereo images and external DEM in spatial resolution and the uncertainty of forest canopy height contained in external DEM. To cope with these problems, image matching techniques and resample were employed to reduce the errors of generated CHM. Fig. 5(a) and (b) illustrated that the directly estimated CHM were significantly smaller than ground measured average height in sample scale, because external DEM contained partial forest canopy height. By correcting the approach with ground measured average height, the rRMSE were ranged from 15.4% to 25.9% for Larch and from 21.6% to 27.1% for Chinese pine, respectively. Furthermore, the Larch forest had already begun to shed leaves at the time of acquired images, so, the CCHM of Larch was more accurate than Chinese pine. However, because of the lower spatial resolution of stereo images, the precision of derived CHM from ZY-3 is still lower than that derived from other platforms, such as worldview-2 and GeoEye-1.

Even so, by adding the CHM, the estimated GSV was obviously improved using four models with three methods of variable selection (see Fig. 6 and Table IV). Comparing with the values of rRMSE and determination coefficient (R^2), it is found that the capability of single CHM for estimating GSV is significantly stronger than the combined Mul-SP variables. Moreover, for combining the Mul-SP variables with CCHM, the values of rRMSE were decreased from 29.3% to 25% for Larch and from 26.5% to 22.2% for Chinese pine. In previous studies, the values of rRMSE were up to 29.8% for Larch and 24.9% for Chinese pine using Sentinel-2 multispectral data in Wangyedian forest [55]. Meanwhile, the values of rRMSE were also reached 27.1% for Larch and 24.9% for Chinese pine using GF-2 multispectral data [50]. It is proved that the CHM extracted from open-sourced DEM has great potential capability to improve the accuracy of estimated GSV by combining Mul-SP variables.

B. Saturation Values of GSV

At present, the optical RS images are widely used to estimate the forest GSV, and the under-estimated GSV is often occurred

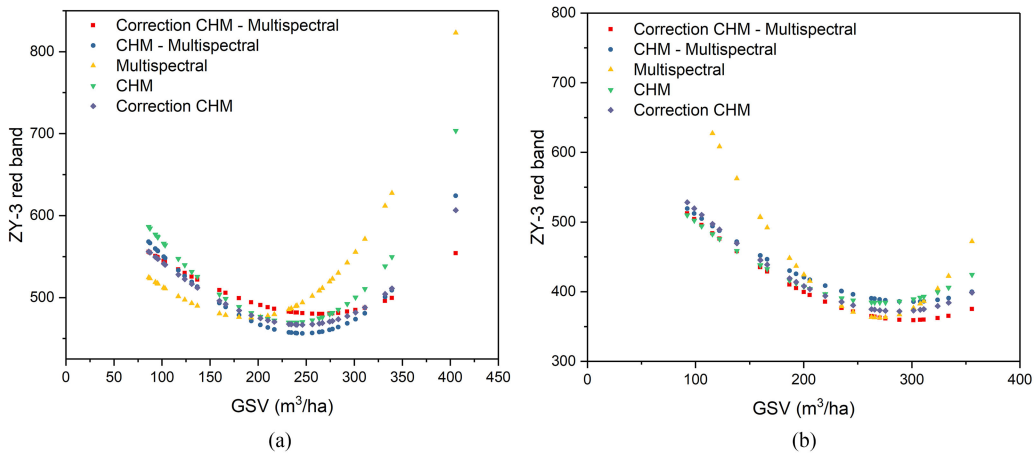

Fig. 9. Curves of spherical model for Larch and Chinese pine. (a) Curves of Larch. (b) Curves of Chinese pine.

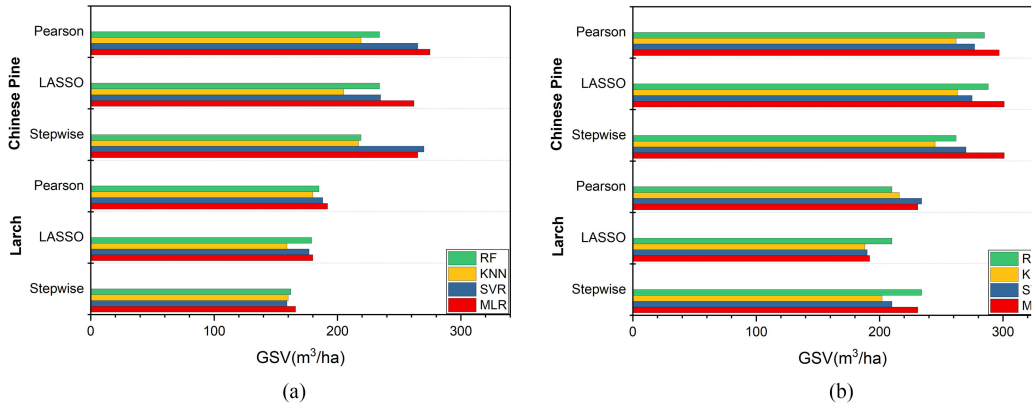

Fig. 10. Levels of saturation derived from different models using Mul-SP and Mul-SP-CCHM. (a) Saturation levels from Mul-SP. (b) Saturation levels from Mul-SP-CCHM.

TABLE V
SATURATION LEVELS OF VARIOUS COMBINED VARIABLES FROM THE OPTIMAL ESTIMATED GSV

Variable	Larch			Chinese pine			Note
	Variable selection	model	Saturation level (m^3/ha)	Variable selection	model	Saturation level(m^3/ha)	
Red band	-	-	150	-	-	220	single
Mul-SP	Pearson	MLR	192	Pearson	MLR	270	combined
CHM	-	linear	231	-	linear	275	single
C CHM	-	linear	246	-	linear	288	single
Mul-SP-CHM	Pearson	SVR	234	Stepwise regression	MLR	301	combined
Mul-SP-CCHM	Pearson	SVR	266	LASSO	KNN	307	combined

caused by saturation of variables. Commonly, the saturation levels of GSV are related to the spectral reflection with various RS images and tree species [14], [25]. To analyze the capability of variables, several approaches were applied to quantitatively determine the saturation levels in the previous study. Using the proposed model, it is easy to determine the saturation levels of combined variables for Larch and Chinese pine (see Fig. 10).

Although the saturation levels of each combined variables from ZY-3 stereo and Mul-SP images were determined by spherical model (see Fig. 10), and the determined saturation levels contained two parts caused by the strategy of evaluation saturation levels. The first part is mainly caused by combined variables, and the other part was introduced by employed estimated models and the methods of variable selection. So, for the same combined variables, the saturation values varied with the methods of variable selection and employed models (see Fig. 10), and the highest and lowest saturation levels were derived from MLR and KNN for Chinese pine and Larch, respectively. In fact, it is difficult to remove the influences of employed models for evaluating the combined variables. Furthermore, the

contribution of CHM for increasing the levels of saturation is larger than Mul-SP variables. Table V and Fig. 10 illustrate that the saturation levels of single CHM were significantly higher than combined variables, and the CHM from stereo images is more sensitive than the spectral variables. After adding the CHM, the averaged saturation levels of the combined variables were increased from 220 m^3/ha to nearly 300m^3/ha for Chinese pine and from 150 to 220 m^3/ha for Larch, respectively.

V. Conclusion

This research confirmed a great potential capability of ZY-3 stereo and Mul-SP images for improvement of the forest GSV by increasing the levels of saturation. Using three high-resolution panchromatic cameras, the CHM was derived from ZY-3 stereo images with subtracting open-sourced external DEM, and 49 alternative variables were extracted from ZY-3 Mul-SP images. After that, CCHM was inverted by ground measured average heights of plots and selected spectral variables, and the underestimated heights of plots were significantly decreased. This research revealed that in the absence of high precision DEM, the reliable CHM can be derived from ZY-3 stereo and Mul-SP images. Moreover, for combining the Mul-SP variables with CCHM, the values of rRMSE for estimating GSV were decreased from 29.3% to 25% for Larch and from 26.5% to 22.2% for Chinese pine, respectively. Meanwhile, the spherical model was employed to determine the saturation levels of combined variables. The validation results showed that the accuracy of estimated forest GSV is highly dependent on the saturation levels and the values of saturation were increased by adding CHM. The results showed that the averaged saturation levels of the combined variables were increased from 220 m^3/ha to nearly 300 m^3/ha for Chinese pine and from 150 to 220 m^3/ha for Larch after adding the CHM, respectively. However, the estimated saturation levels employed the spherical model induced by the combined variable set and employed models. It is needed to further research for separation of the effects from the employed models.

References

[1] Y. Pan, R. A. Birdsey, O. L. Phillips, and R. B. Jackson, "The structure, distribution, and biomass of the world's forests," *Annu. Rev. Ecol., Evol., Systematics,* vol. 44, pp. 593–622, 2013.

[2] J.-M. Carnus *et al.*, "Planted forests and biodiversity," *J. Forestry,* vol. 104, no. 2, pp. 65–77, 2006.

[3] T. Wang, F. Kang, H. Han, X. Cheng, J. Zhu, and W. Zhou, "Estimation of leaf area index from high resolution ZY-3 satellite imagery in a catchment dominated by larix principis-rupprechtii, northern China," *J. Forestry Res.,* vol. 30, no. 2, pp. 603–615, 2019.

[4] I. Balenović, A. Simic Milas, and H. Marjanović, "A comparison of stand-level volume estimates from image-based canopy height models of different spatial resolutions," *Remote Sens.,* vol. 9, no. 3, 2017, Art. no. 205.

[5] S. Puliti, S. Saarela, T. Gobakken, G. Ståhl, and E. Næsset, "Combining UAV and sentinel-2 auxiliary data for forest growing stock volume estimation through hierarchical model-based inference," *Remote Sens. Environ.,* vol. 204, pp. 485–497, 2018.

[6] S. Wittke, X. Yu, M. Karjalainen, J. Hyyppä, and E. Puttonen, "Comparison of two-dimensional multitemporal sentinel-2 data with three-dimensional remote sensing data sources for forest inventory parameter estimation over a boreal forest," *Int. J. Appl. Earth Observ. Geoinf.,* vol. 76, pp. 167–178, 2019.

[7] P. Singh and R. D. Garg, "Classification of high resolution satellite images using spatial constraints-based fuzzy clustering," *J. Appl. Remote Sens.,* vol. 8, no. 1, 2014, Art. no. 083526.

[8] P. P. Singh and R. Garg, "Fixed point ICA based approach for maximizing the non-Gaussianity in remote sensing image classification," *J. Indian Soc. Remote Sens.,* vol. 43, no. 4, pp. 851–858, 2015.

[9] M. J. Falkowski, M. A. Wulder, J. C. White, and M. D. Gillis, "Supporting large-area, sample-based forest inventories with very high spatial resolution satellite imagery," *Prog. Phys. Geogr.,* vol. 33, no. 3, pp. 403–423, 2009.

[10] S. Zheng *et al.*, "Retrieval of forest growing stock volume by two different methods using landsat TM images," *Int. J. Remote Sens.,* vol. 35, no. 1, pp. 29–43, 2014.

[11] I. Chrysafis, G. Mallinis, S. Siachalou, and P. Patias, "Assessing the relationships between growing stock volume and sentinel-2 imagery in a mediterranean forest ecosystem," *Remote Sens. Lett.,* vol. 8, no. 6, pp. 508–517, 2017.

[12] F. L. Macedo, A. M. Sousa, A. C. Gonçalves, J. R. Marques da Silva, P. A. Mesquita, and R. A. Rodrigues, "Above-ground biomass estimation for quercus rotundifolia using vegetation indices derived from high spatial resolution satellite images," *Eur. J. Remote Sens.,* vol. 51, no. 1, pp. 932–944, 2018.

[13] G. Li, Z. Xie, X. Jiang, D. Lu, and E. Chen, "Integration of Ziyuan-3 multispectral and stereo data for modeling aboveground biomass of larch plantations in north China," *Remote Sens.,* vol. 11, no. 19, 2019, Art. no. 2328.

[14] P. Zhao, D. Lu, G. Wang, C. Wu, Y. Huang, and S. Yu, "Examining spectral reflectance saturation in landsat imagery and corresponding solutions to improve forest aboveground biomass estimation," *Remote Sens.,* vol. 8, no. 6, 2016, Art. no. 469.

[15] O. W. Tsui, N. C. Coops, M. A. Wulder, and P. L. Marshall, "Integrating airborne LiDAR and space-borne radar via multivariate kriging to estimate above-ground biomass," *Remote Sens. Environ.,* vol. 139, pp. 340–352, 2013.

[16] D. Lu *et al.*, "Aboveground forest biomass estimation with landsat and LiDAR data and uncertainty analysis of the estimates," *Int. J. Forestry Res.,* vol. 2012, 2012, Art. no. 436537.

[17] N. Joshi *et al.*, "Understanding 'saturation'of radar signals over forests," *Sci. Rep.,* vol. 7, no. 1, pp. 1–11, 2017.

[18] M. Cutler, D. Boyd, G. Foody, and A. Vetrivel, "Estimating tropical forest biomass with a combination of SAR image texture and landsat TM data: An assessment of predictions between regions," *ISPRS J. Photogram. Remote Sens.,* vol. 70, pp. 66–77, 2012.

[19] A. A. Dos Reis, S. E. Franklin, J. M. de Mello, and F. W. Acerbi Junior, "Volume estimation in a eucalyptus plantation using multi-source remote sensing and digital terrain data: A case study in Minas Gerais State, Brazil," *Int. J. Remote Sens.,* vol. 40, no. 7, pp. 2683–2702, 2019.

[20] H. Zhang *et al.*, "Forest growing stock volume estimation in subtropical mountain areas using PALSAR-2 L-band PolSAR data," *Forests,* vol. 10, no. 3, 2019, Art. no. 276.

[21] M. S. Ataee, Y. Maghsoudi, H. Latifi, and F. Fadaie, "Improving estimation accuracy of growing stock by multi-frequency SAR and multi-spectral data over Iran's heterogeneously-structured broadleaf Hyrcanian forests," *Forests,* vol. 10, no. 8, 2019, Art. no. 641.

[22] M. Mura *et al.*, "Exploiting the capabilities of the sentinel-2 multi spectral instrument for predicting growing stock volume in forest ecosystems," *Int. J. Appl. Earth Observ. Geoinf.,* vol. 66, pp. 126–134, 2018.

[23] R. E. McRoberts, E. Næsset, and T. Gobakken, "Inference for lidar-assisted estimation of forest growing stock volume," *Remote Sens. Environ.,* vol. 128, pp. 268–275, 2013.

[24] D. Lu, Q. Chen, G. Wang, L. Liu, G. Li, and E. Moran, "A survey of remote sensing-based aboveground biomass estimation methods in forest ecosystems," *Int. J. Digit. Earth,* vol. 9, no. 1, pp. 63–105, 2016.

[25] D. Lu, "The potential and challenge of remote sensing-based biomass estimation," *Int. J. Remote Sens.,* vol. 27, no. 7, pp. 1297–1328, 2006.

[26] T. Dube and O. Mutanga, "Investigating the robustness of the new landsat-8 operational land imager derived texture metrics in estimating plantation forest aboveground biomass in resource constrained areas," *ISPRS J. Photogram. Remote Sens.*, vol. 108, pp. 12–32, 2015.

[27] J. Long, H. Lin, G. Wang, H. Sun, and E. Yan, "Mapping growing stem volume of chinese fir plantation using a saturation-based multivariate method and Quad-polarimetric SAR images," *Remote Sens.,* vol. 11, no. 16, pp. 1872, 2019.

[28] Y. Hu *et al.*, "Estimating forest stock volume in Hunan province, China, by integrating in situ plot data, sentinel-2 images, and linear and machine learning regression models," *Remote Sens.,* vol. 12, no. 1, 2020, Art. no. 186.
[29] G. S. A. de Souza *et al.*, "Multi-sensor prediction of eucalyptus stand volume: A support vector approach," *ISPRS J. Photogram. Remote Sens.,* vol. 156, pp. 135–146, 2019.
[30] L. Breiman, "Random forests," *Mach. Learn.,* vol. 45, no. 1, pp. 5–32, 2001.
[31] M. I. Sameen, B. Pradhan, D. T. Bui, and A. M. Alamri, "Systematic sample subdividing strategy for training landslide susceptibility models," *Catena,* vol. 187, 2020, Art. no. 104358.
[32] T. Dube, O. Mutanga, E. M. Abdel-Rahman, R. Ismail, and R. Slotow, "Predicting eucalyptus spp. stand volume in Zululand, South Africa: An analysis using a stochastic gradient boosting regression ensemble with multi-source data sets," *Int. J. Remote Sens.,* vol. 36, no. 14, pp. 3751–3772, 2015.
[33] R. E. McRoberts, T. Gobakken, and E. Næsset, "Post-stratified estimation of forest area and growing stock volume using lidar-based stratifications," *Remote Sens. Environ.,* vol. 125, pp. 157–166, 2012.
[34] B. Koch, "Status and future of laser scanning, synthetic aperture radar and hyperspectral remote sensing data for forest biomass assessment," *ISPRS J. Photogram. Remote Sens.,* vol. 65, no. 6, pp. 581–590, 2010.
[35] J. Boudreau, R. F. Nelson, H. A. Margolis, A. Beaudoin, L. Guindon, and D. S. Kimes, "Regional aboveground forest biomass using airborne and spaceborne LiDAR in Québec," *Remote Sens. Environ.,* vol. 112, no. 10, pp. 3876–3890, 2008.
[36] V. Giannico, R. Lafortezza, R. John, G. Sanesi, L. Pesola, and J. Chen, "Estimating stand volume and above-ground biomass of urban forests using LiDAR," *Remote Sens.,* vol. 8, no. 4, 2016, Art. no. 339.
[37] K. Ioki, J. Imanishi, T. Sasaki, Y. Morimoto, and K. Kitada, "Estimating stand volume in broad-leaved forest using discrete-return lidar: Plot-based approach," *Landscape Ecological Eng.,* vol. 6, no. 1, 2010, Art. no. 29.
[38] P. Watt and M. S. Watt, "Development of a national model of pinus radiata stand volume from LiDAR metrics for New Zealand," *Int. J. Remote Sens.,* vol. 34, no. 16, pp. 5892–5904, 2013.
[39] C. Thiel and C. Schmullius, "The potential of ALOS PALSAR backscatter and InSAR coherence for forest growing stock volume estimation in Central Siberia," *Remote Sens. Environ.,* vol. 173, pp. 258–273, 2016.
[40] M. Santoro, L. Eriksson, J. Askne, and C. Schmullius, "Assessment of stand-wise stem volume retrieval in boreal forest from JERS-1 L-band SAR backscatter," *Int. J. Remote Sens.,* vol. 27, no. 16, pp. 3425–3454, 2006.
[41] G. Goldbergs, S. W. Maier, S. R. Levick, and A. Edwards, "Limitations of high resolution satellite stereo imagery for estimating canopy height in australian tropical savannas," *Int. J. Appl. Earth Observ. Geoinf.,* vol. 75, pp. 83–95, 2019.
[42] W. Ni, Z. Zhang, G. Sun, and Q. Liu, "Modeling the stereoscopic features of mountainous forest landscapes for the extraction of forest heights from stereo imagery," *Remote Sens.,* vol. 11, no. 10, 2019, Art. no. 1222.
[43] O. Antropov, Y. Rauste, T. Häme, and J. Praks, "Polarimetric ALOS PALSAR time series in mapping biomass of boreal forests," *Remote Sens.,* vol. 9, no. 10, 2017, Art. no. 999.
[44] R. K. Ningthoujam *et al.*, "Relationships of S-band radar backscatter and forest aboveground biomass in different forest types," *Remote Sens.,* vol. 9, no. 11, 2017, Art. no. 1116.
[45] B. H. Trisasongko, "Mapping stand age of rubber plantation using ALOS-2 polarimetric SAR data," *Eur. J. Remote Sens.,* vol. 50, no. 1, pp. 64–76, 2017.
[46] W. Wagner *et al.*, "Large-scale mapping of Boreal forest in SIBERIA using ERS tandem coherence and JERS backscatter data," *Remote Sens. Environ.,* vol. 85, no. 2, pp. 125–144, 2003.
[47] Z. Xie, Y. Chen, D. Lu, G. Li, and E. Chen, "Classification of land cover, forest, and tree species classes with ZiYuan-3 multispectral and stereo data," *Remote Sens.,* vol. 11, no. 2, 2019, Art. no. 164.
[48] Y. Xu, C. Li, Z. Sun, L. Jiang, and J. Fang, "Tree height explains stand volume of closed-canopy stands: Evidence from forest inventory data of China," *Forest Ecol. Manage.,* vol. 438, pp. 51–56, 2019.
[49] Y. Li, M. Li, Z. Liu, and C. Li, "Combining kriging interpolation to improve the accuracy of forest aboveground biomass estimation using remote sensing data," *IEEE Access,* vol. 8, pp. 128124–128139, 2020.
[50] X. Li *et al.*, "Estimating the growing stem volume of Chinese pine and larch plantations based on fused optical data using an improved variable screening method and stacking algorithm," *Remote Sens.,* vol. 12, no. 5, 2020, Art. no. 871.
[51] X. Li, J. Long, M. Zhang, Z. Liu, and H. Lin, "Coniferous plantations growing stock volume estimation using advanced remote sensing algorithms and various fused data," *Remote Sens.,* vol. 13, no. 17, 2021, Art. no. 3468.
[52] X. Li, M. Zhang, J. Long, and H. Lin, "A novel method for estimating spatial distribution of forest above-ground biomass based on multispectral fusion data and ensemble learning algorithm," *Remote Sens.,* vol. 13, no. 19, 2021, Art. no. 3910.
[53] D. E. Shean *et al.*, "An automated, open-source pipeline for mass production of digital elevation models (DEMs) from very-high-resolution commercial stereo satellite imagery," *ISPRS J. Photogram. Remote Sens.,* vol. 116, pp. 101–117, 2016.
[54] P. M. Montesano, C. Neigh, G. Sun, L. Duncanson, J. Van Den Hoek, and K. J. Ranson, "The use of sun elevation angle for stereogrammetric boreal forest height in open canopies," *Remote Sens. Environ.,* vol. 196, pp. 76–88, 2017.
[55] F. Jiang *et al.*, "Estimating the growing stem volume of coniferous plantations based on random forest using an optimized variable selection method," *Sensors,* vol. 20, no. 24, 2020, Art. no. 7248.
[56] G. J. Székely, M. L. Rizzo, and N. K. Bakirov, "Measuring and testing dependence by correlation of distances," *Ann. Statist.,* vol. 35, no. 6, pp. 2769–2794, 2007.
[57] M. A. Oliver and R. Webster, "Kriging: A method of interpolation for geographical information systems," *Int. J. Geographical Inf. Syst.,* vol. 4, no. 3, pp. 313–332, 1990.
[58] F. Danson and S. Plummer, "Red-edge response to forest leaf area index," *Remote Sens.*, vol. 16, no. 1, pp. 183–188, 1995.
[59] D. Lu, P. Mausel, E. Brondızio, and E. Moran, "Relationships between forest stand parameters and landsat TM spectral responses in the Brazilian Amazon basin," *Forest Ecol. Manage.,* vol. 198, no. 1–3, pp. 149–167, 2004.
[60] V. O. Zharko, S. A. Bartalev, and V. M. Sidorenkov, "Forest growing stock volume estimation using optical remote sensing over snow-covered ground: A case study for Sentinel-2 data and the Russian Southern Taiga region," *Remote Sens. Lett.,* vol. 11, no. 7, pp. 677–686, 2020.

Tingchen Zhang was born in Alxa, Inner Mongolia, China, in 1997. He received the B.S. degree in agriculture from Central South University of Forestry and Technology, Changsha, China, in 2019, where he is currently working toward the M.S. degree in forest management.

His current research interest focuses on the application of photogrammetry to remote sensing monitoring in forest.

Hui Lin was born in Huanggang, Hubei Province, China, in 1965. She received the Ph.D. degree in agronomy from Central South University of Forestry and Technology, Changsha, China, in 2016.

She is currently a Professor and Doctoral Supervisor with Central South University of Forestry and Technology, Deputy Director of Forestry Remote Sensing Information Engineering Research Center, and Director of Hunan Provincial Key Laboratory of Forestry Remote Sensing Big Data and Ecological Security. She is mainly engaged in the teaching and research of forest management, forestry remote sensing, and geographic information system.

Jiangping Long was born in Changde, Hunan province, China. He received the M.S. and Ph.D. degrees in engineering from Central South University, Changsha, China, in 2017 and 2020 respectively.

He is currently an Associate Professor with Central South University of Forestry and Technology, Changsha, China. His current research interest include high-resolution remote sensing image processing, microwave remote sensing and surface deformation monitoring, polar-polarized SAR data processing, and forest parameters inversion.

Meng Zhang was born in Yueyang, Hunan province, China in 1987. He received the Ph.D. degree in engineering from Central South University, Changsha, China, in 2018.

He is currently a Lecturer with Central South University of Forestry and Technology, Changsha, China. His current research interests include remote sensing of resources and environment, remote sensing of wetland ecology, and application of geographic information system.

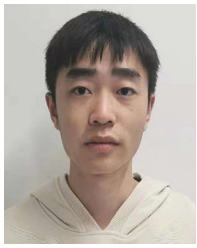

Zhaohua Liu was born in Mudanjiang, Heilongjiang province, China, in 1994. He received the B.S. and M.S. degrees in agriculture from Central South University of Forestry and Technology, Changsha, China, in 2017 and 2020 respectively. He is currently working toward the Ph.D. degree in forest management with Central South University of Forestry and Technology.

His current research interests include remote sensing information processing and quantitative remote sensing of forest parameters.